55

HIGH ENERGY EMISSION IN SEYFERT GALAXY IC 4329A

OBSERVATIONS: G. MADEJSKI, et al.

THEORY: A. ZDZIARSKI, et al.

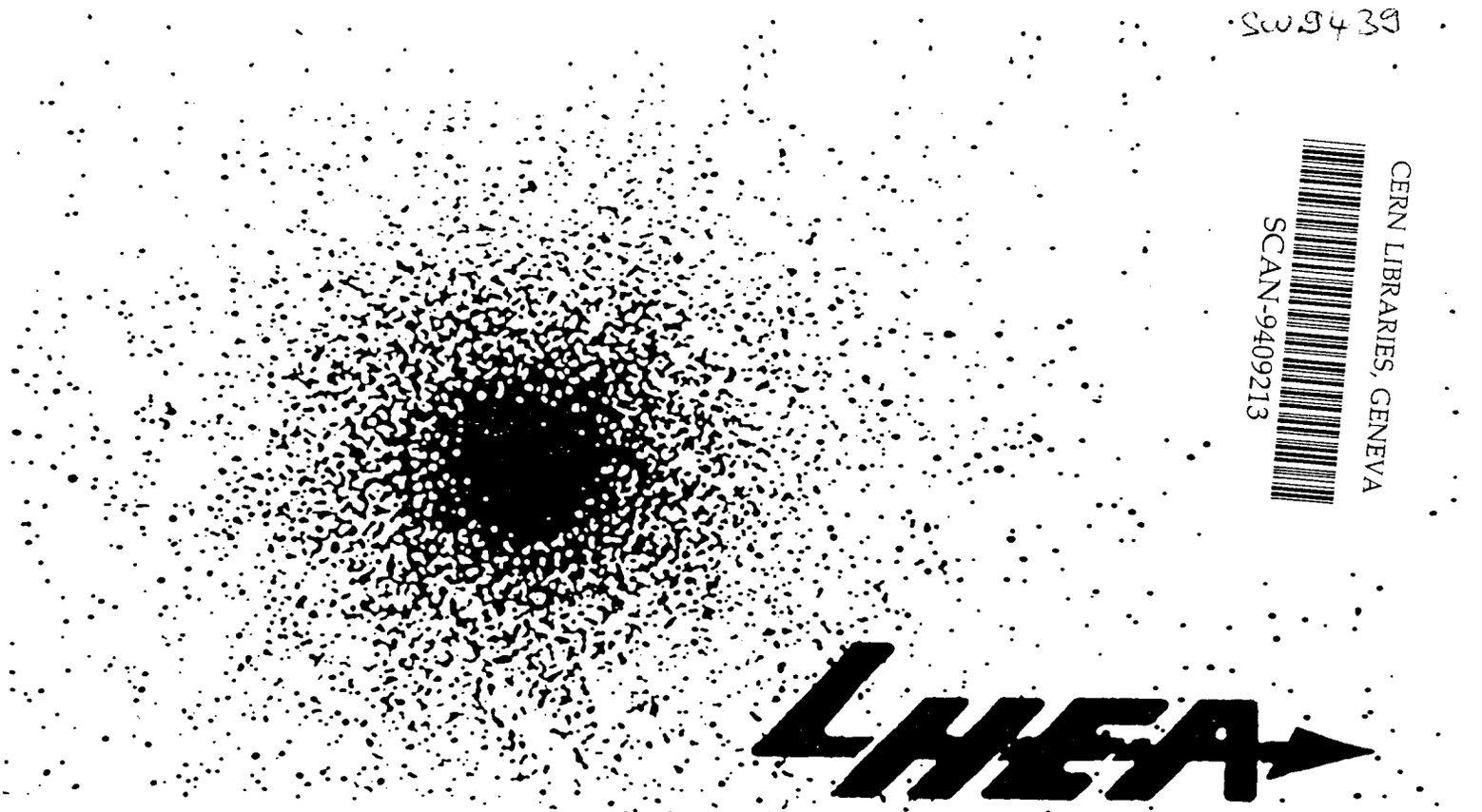

LABORATORY FOR HIGH ENERGY ASTROPHYSICS

National Aeronautics And Space Administration
Goddard Space Flight Center
Greenbelt, Maryland 20771

X-ray: 94-9/10

HIGH ENERGY EMISSION IN SEYFERT GALAXY IC 4329A

OBSERVATIONS: G. Madejski et al. (accepted for publication in ApJ)

THEORY: A. Zdziarksi et al. (accepted for publication in MNRAS)

Code 666
X-ray Astrophysics Branch
Laboratory for High Energy Astrophysics
NASA/Goddard Space Flight Center
Greenbelt, Maryland 20771 USA

Joint ROSAT - Compton GRO Observations of the X-ray Bright Seyfert Galaxy IC 4329A

G. M. Madejski[1,2], A. A. Zdziarski[3], T. J. Turner[1,2], C. Done[4], R. F. Mushotzky[1], R. C. Hartman[1], N. Gehrels[1], A. Connors[5], A. C. Fabian[6], K. Nandra[6], A. Celotti[6], M. J. Rees[6], W. N. Johnson[7], J. E. Grove[7], and C. H. Starr[1,7,8]

[1]Lab for High Energy Astrophysics, NASA/Goddard, Greenbelt, MD 20771
[2]With Universities Space Research Association
[3]N. Copernicus Astronomical Center, Bartycka 18, 00-716 Warsaw, Poland
[4]The Physics Dept., Leicester University, UK
[5]Space Science Center, Univ. of New Hampshire, Durham, NH 03824
[6]Institute of Astronomy, Cambridge University, Cambridge, UK
[7]E. O. Hulburt Center for Space Research, Naval Research Lab, Washington, DC 20375
[8]Science Programs, Computer Sciences Corporation, Calverton, MD 20705

Accepted for publication in the Astrophysical Journal

ABSTRACT

We report a simultaneous *ROSAT* and *GRO* observation of the X-ray bright Seyfert galaxy IC 4329A. For the *GRO* OSSE detector, we also present the sum of the data for this and earlier observations. The overall spectrum is very well described as a power law with an energy spectral index of ~ 1 absorbed at low energies plus a strong Compton reflection component, typical for Seyfert 1 galaxies. The low energy absorption can be well described by a sum of a neutral column density of $\sim 3 \times 10^{21}$ cm^{-2}, most of which is associated with the edge-on galactic disk of IC 4329A, plus an edge-like feature at ~ 700 eV; this feature implies either complex absorption (due to additional ionized material, or due to partial covering), or a soft excess. The data only weakly constrain the presence of a high-energy cutoff in the underlying power law; they are compatible with an exponential cutoff at any energy $E_C \gtrsim 100$ keV. The relative steepness of the OSSE data, with the power law energy index of 1.6 ± 0.2, can be accounted for entirely by the contribution of the high-energy tail of the reflection component when $E_C \to \infty$. (We find that the definite cutoff at an energy $E_C \sim 130$ keV suggested in the recently published analysis of the OSSE data for this object is due to a data reduction error.) Including non-simultaneous *Ginga* observations with 2 keV fluxes matching well that of *ROSAT* gives us likely broad-band X-ray/γ-ray spectra of the object from ~ 0.1 keV up to several hundred keV. Joint spectral analysis of the data sets from the three instruments gives results similar to those from *ROSAT*/OSSE only, except that the cutoff energy is now constrained to be at 250 keV $\lesssim E_C \lesssim 1700$ keV. The constraint on E_C markedly distinguishes this object from NGC 4151, where E_C was lower, ~ 50 keV; this has implications for emission models for AGN as well as for their contribution to the X-ray background.

We also report the *ROSAT* spectrum of the companion object to the Seyfert, the elliptical galaxy IC 4329 located $\sim 3'$ away. Its spectrum is well described by an optically thin thermal plasma with $kT = 0.9$ keV, with a 0.1–2 keV flux of 8×10^{-13} ergs cm^{-2} s^{-1}, corresponding to a luminosity of $\sim 8 \times 10^{41}$ ergs s^{-1}.

Subject headings: galaxies: individual (IC 4329A, IC 4329) — galaxies: Seyfert — X-rays: galaxies — gamma rays: observations

1. INTRODUCTION

The nature of high energy emission from AGNs is still not understood. That is due to the lack of sensitivity of instruments at high energies, where good data would constrain theoretical models more tightly. So far, the best studied object has been the one brightest in hard X-rays, NGC 4151. However, we are certain that its X-ray emission is unique as compared to the majority of Seyfert 1s: the 2–20 keV X-ray spectrum of this rather low luminosity object is unusually flat, with a power law index α (defined via the energy flux $F_E \propto E^{-\alpha}$) of 0.3–0.7 (e.g., Yaqoob et al. 1993), quite different than $\alpha \simeq 0.9$–1, characteristic for the power law components of bright Seyfert 1s (Pounds et al. 1990; Nandra & Pounds 1994). So, extending any inferences to Seyfert 1s as a class, e.g., with regard to the emission mechanisms or their contribution to the X-ray background, on the basis of the X-ray and soft γ-ray spectrum of NGC 4151 is probably premature and possibly misleading.

The second brightest hard X-ray Seyfert, IC 4329A ($F_{2-10\ \mathrm{keV}} \simeq 2 \times 10^{-10}$ ergs cm^{-2} s^{-1}), is likely to be more representative of Seyfert 1s as a class. It is a relatively nearby ($z = 0.0157$; Wilson & Penston 1979), luminous object. The X-ray spectrum of it is typical for Seyfert 1s, with a power law component with $\alpha \simeq 1$ (Piro, Yamauchi, & Matsuoka 1990) as well as a component due to reflection of the power law by cold matter (Lightman & White 1988). IC 4329A thus holds a promise to assess the general applicability of theoretical AGN models, e.g., those developed for NGC 4151 (e.g., Zdziarski, Lightman, & Maciołek-Niedźwiecki 1993). We find that the line-of-sight absorption (seen in the *ROSAT* data) due to the host galaxy oriented edge-on is not large enough to affect studies of the X-ray continuum.

X-ray emission in Seyferts is generally variable, and constraining of any models attempting to explain broad-band spectra requires simultaneous observations by several satellites. While in comparison to other Seyferts, IC 4329A varies only modestly, $\pm 50\%$ (Halpern 1982), this variability is strong enough to make simultaneous observations critical for testing theoretical models. To that end, we scheduled our *ROSAT* and *GRO* observations (including those by the OSSE, previously reported by Fabian et al. 1993, hereafter F93) to be simultaneous. This gives us perhaps the broadest-band simultaneous observation of any radio-quiet AGN obtained yet, and we present it below. We find, however, that due to a gap between 2 and 50 keV the confidence regions on spectral parameters are rather large. We can constrain those parameters much more tightly if we use the *Ginga* data (analyzed in Fiore et al. 1992, hereafter F92) that turn out to match the 2 keV *ROSAT* flux very closely. As spectral variations of the object are weak (F92), it is likely that the resulting broad-band spectrum is close to a true simultaneous X-ray/γ-ray spectrum of the object.

2. DATA

2.1. The ROSAT Observation

The data reported here are from an observation nominally centered at the optical position of IC 4329A, which is at R. A. (2000.0) = $13^h49^m19.2^s$, Dec (2000.0) = $-30°18'34''$. The observation was performed over the period 1993 Jan 14 11:41–18:46 UT using the *ROSAT* X-Ray Telescope with the PSPC-B in the focal plane, sensitive over 0.1–2.4 keV, with the FWHM energy resolution of $\Delta E/E = 0.43(E_{\mathrm{keV}}/0.93)^{-0.5}$. The total on-source exposure time was 8230 seconds. The data, collected with the spacecraft "wobble" turned on, were processed using the SASS v. 6.2 and PROS v. 2.10. All subsequent spectral fitting used the 93 Jan 12 PSPC-B resolution matrix.

The X–ray image of the field containing IC 4329A is shown in Fig. 1. IC 4329A is the nearly on-axis (within the $\sim 10''$ nominal *ROSAT* pointing error) source in the PSPC image, at R. A. (2000.0) = $13^h49^m19.5^s$, Dec (2000.0) = $-30°18'27.3''$; its image is consistent with being point-like. Besides IC 4329A, several other sources are present (see Fig. 1), and two show the PSPC count rate greater than 1/100 of that of IC 4329A. The source at $\sim 3'$ away, at R. A. (2000.0) = $13^h49^m5.8^s$, Dec (2000.0) = $-30°17'38.5''$ is within $\sim 10''$ of the optical position of IC 4329, a companion galaxy

to IC 4329A, and is likely to be that galaxy indeed. A third source is located about 12′ away, at R. A. (2000.0) = $13^h48^m44.5^s$, Dec (2000.0) = $-30°29'32.5''$ (where the positional error may be slightly larger, $\sim 20''$, due to its off-axis location); we will subsequently call this source S3. We extracted spectra of all 3 objects from within a 3′ (for IC 4329A and S3) and 1.6′ (for IC 4329) radius circles around the centroid of each source. The background counts corresponding to IC 4329A and S3 were collected from annuli centered on the sources, with inner radius of 5′ and outer radius of 10′, avoiding regions containing any other source. For IC 4329, we selected a background region on the opposite side of IC 4329A, at the same radial distance from it as IC 4329, such that the source and background cells contained the same contamination from the brighter source, such as to subtract away any residual counts due to IC 4329A. The resulting net count rates in the 0.1–2 keV band from IC 4329A, IC 4329, and S3 were respectively $2.65 \pm 0.02, 0.081 \pm 0.004$, and 0.086 ± 0.006 counts s^{-1}. To allow for residual PSPC calibration errors, we added in quadrature a systematic error of 2% to the statistical error on the count rate for each channel.

2.2. The GRO Observations

IC 4329A was observed by OSSE on the *GRO* during three viewing periods: 41: 1992 Oct. 8 – Oct. 15, 44: 1992 Nov. 3 – Nov. 17, and 207: 1993 Jan. 12 – Feb. 2. The last of these observations (covering the *ROSAT* observation) was described by F93. During this analysis, we have corrected an effective area error in the earlier analysis of the OSSE data, which essentially only affects the conversion of normalization from the count rate to flux. We also have added the data from the earlier, 1992 Oct. and 1992 Nov. observations. The observation and analysis techniques for all data were discussed in F93. After correcting the 1993 OSSE data in F93 for a factor of 4 effective area mistake, the results for the combined data as presented here are in agreement with the 1993 data alone. The average OSSE fluxes in the 50–150 keV band for the three periods are: $5.7 \pm 1.5, 7.4 \pm 0.9$, and 7.8 ± 0.6, in units of 10^{-4} photons cm^{-2} s^{-1}, for viewing periods, 41, 44, and 207 respectively.

During the 1993 Jan. 12–Feb. 2 GRO observing period, the source was also observed by the COMPTEL and EGRET instruments, but it was not detected. The 2-σ COMPTEL upper limits for the viewing period 207 are 7.4, 11, 5.2, and 2.0 in units of 10^{-5} photons cm^{-2} s^{-1} over bands of, respectively, 0.75–1, 1–3, 3–10, and 10–30 MeV. The EGRET 0.1–30 GeV upper limits are 1.6×10^{-7} and 4.9×10^{-8} photons s^{-1} cm^{-2} for the viewing period 207 and for all EGRET observations of this object, respectively.

3. SPECTRAL FITTING

3.1. Spectrum of IC 4329A

The main objective of the *ROSAT* part of the coordinated *ROSAT*/*GRO* observations of IC 4329A was to establish the flux level in the soft X-rays. At the time of our joint observations, there were no functioning observatories sensitive in the bandpass between the high-energy cutoff of *ROSAT* and the low-energy cutoff of OSSE, so we compared our data with non-simultaneous 2–25 keV *Ginga* data. This object was observed for three days with *Ginga* in 1989 (Piro et al. 1990; F92), when it was seen to vary by $\sim 25\%$ in flux. Spectral changes, if any, were modest, and all three spectra are consistent with the same spectral shape (F92). Our comparison of *ROSAT* and *Ginga* data revealed that the 2 keV fluxes of the data from 1989 July 8 and 9 are virtually identical with that of *ROSAT*. On the other hand, the *Ginga* flux for 1989 July 10 was about 25% higher. Thus, we used the 1989 July 8, 9 data in joint fits for all three instruments.

3.1.1. ROSAT spectrum of IC 4329A

We present the spectral fits to the *ROSAT* observation alone in Table 1. The data can be adequately described by a simple power law with the best fit parameters of $\alpha = 0.15 \pm 0.18$, absorbed by a column of $N_{\rm H} = (2.0 \pm 0.3) \times 10^{21}$ cm^{-2}. (All errors are given for 90% confidence for one parameter of interest, i.e., $\Delta\chi^2 = 2.7$.) The data and residuals are presented in Figure

2. However, even though the χ^2 is acceptable (46.1/44 d.o.f.), inspection of the residuals shows an edge-like feature at $\sim$ 700 eV. Incorporating an edge into the model improves the statistics to χ^2 = 30.3/42 d.o.f. and it gives $\alpha = 0.83 \pm 0.4$, consistent with the spectral index observed by *Ginga*, $\alpha \simeq 1.0$; $N_{\rm H}$ is now $(3.0 \pm 0.8) \times 10^{21}$ cm^{-2}. The data and residuals for this model are given in Figure 3. The edge energy is $E_{\rm edge} = 0.72 \pm 0.07$ keV and its optical depth is $\tau_{\rm edge} = 0.56 \pm 0.24$. We discuss the possible instrumental effects on the inferred spectral parameters in the Appendix, but we conclude there that the presence of the feature is independent on these effects.

The energy of the edge is inconsistent with that expected from neutral absorber, and implies that it is most likely due to OVI and OVII, which is suggestive of ionized absorber. Therefore, we fitted the data by a power law modified by a sum of neutral and ionized absorbers. We use the XSTAR implementation of the ionized absorber model (with no self-emission), which assumes a single-zone, optically-thin, constant density material, where the temperature is calculated self-consistently, (cf. Krolik and Kallman 1992; see also Done et al. 1992). The ionization parameter ξ is defined as $L/(nr^2)$, where L is the ionizing luminosity between 1 and 1000 Ry, r is the distance from the ionizing source, and n is the gas density (cf. Kallman & McCray 1982). In our fit, we assume $\alpha = 1$, and obtain the neutral column of $2.3 \pm 0.7 \times 10^{21}$ cm^{-2}, plus an ionized column of $(3.8^{+1.4}_{-1.0}) \times 10^{21}$ cm^{-2} with the ionization parameter $\xi = 3.4^{+22}_{-1.6}$; χ^2 is now 30.4/43 d.o.f.

However, the ionized absorber model is not a unique interpretation of the spectral complexity present in the *ROSAT* data, due to the modest energy resolution of the PSPC. An alternative acceptable model is partial covering by neutral material, yielding χ^2 = 32.1/43 d.o.f. for the fixed $\alpha = 1$, with $1.8^{+0.6}_{-0.4} \times 10^{21}$ cm^{-2} covering 100% of the source, with an additional column of $5.1^{+1.8}_{-0.9} \times 10^{21}$ cm^{-2} covering 72^{+8}_{-16}% of the source. We note here that this column is substantially smaller than the partial absorber column of $\sim 2 \times 10^{24}$ cm^{-2} which was invoked as one alternative (next to Compton reflection) to account for the "hump" above $\sim$ 8 keV reported by Piro et al. (1990) on the basis of the *Ginga* data.

It is also possible that the edge-like feature is due to even higher (than 3×10^{21} cm^{-2}) column of cold absorber, with a soft excess (due to, e.g., a tail end of emission from an accretion disk). The soft excess can be modelled as a black body or a power law; fixing the hard power law at $\alpha = 1$ results in χ^2 = 30.9/43 d.o.f. with a black body temperature of 68 ± 10 eV and $N_{\rm H}$ of $4.7 \pm 0.4 \times 10^{21}$ cm^{-2}; a steep power law form of the soft excess (with α_s of 5.0–6.9) is also allowed, but in any case, the intersection with the hard power law must be near 600–700 eV.

Clearly, the modest energy resolution of *ROSAT* does not allow us to distinguish among several models that could describe the spectral structure present in the data. We summarize these models in Table 1. In all cases, the residuals appear nearly identical to these for the absorbed power law + edge model as discussed above. The Galactic $N_{\rm H}$ is only 4.55×10^{20} cm^{-2} (Elvis, Lockman, & Wilkes 1989), so, regardless of the interpretation of the edge, there is a rather substantial amount of cold intrinsic absorption in the line of sight to IC 4329A (as expected given the edge-on orientation of the galaxy; see Petre et al. 1984 for details). We note here that this intrinsic cold absorption is neglected by Nandra & Pounds 1994 in their fit to the *Ginga* spectrum of IC 4329A, yielding a larger ionized column than that inferred here. Regardless of the model, the 0.1–2 keV flux of from IC 4329A is 3×10^{-11} ergs cm^{-2} s^{-1}, with a nominal $\sim$ 10% error due to the absolute effective area calibration uncertainties. The unabsorbed 0.1–2 keV flux (at $\alpha = 1$) varies markedly between the different models, from 8×10^{-11} (partial covering), 1.7×10^{-10} (ionized absorber), and 7×10^{-10} (blackbody) ergs cm^{-2} s^{-1}, respectively. With the ionized absorber, this corresponds to a luminosity of 1.8×10^{44} ergs s^{-1} (H_0 = 50 km s^{-1} Mpc^{-1}).

3.1.2. OSSE spectrum of IC 4329A

The spectral fit parameters to the OSSE data alone during viewing period 207 differ only slightly

(except for the flux, which is now greater by a factor of 4) from those reported in F93. We have used the data up to $\sim$ 1 MeV, as the upper limits for higher energies are above predictions of any plausible model and inclusion of the higher energy data only increases statistical noise. Signal is detected up to $\sim$ 200 keV. A simple power law model fits the data adequately, and yields $\alpha = 1.61^{-0.33}_{+0.38}$ with $\chi^2 = 123/117$ d.o.f. The normalization of the power law at 100 keV is $(5.4 \pm 0.4) \times 10^{-3}$ photons cm^{-2} s^{-1} MeV^{-1}. The limits ($\Delta\chi^2 = 3.84$) on the strength of a Gaussian 511 keV line vary from 4.8 to 10×10^{-5} photons cm^{-2} s^{-1} for the line widths from 5 keV to 350 keV.

The co-added spectrum for all the three viewing periods is virtually identical to that of the period 207; the best fit power law index is $\alpha = 1.60 \pm 0.25$ and the 100 keV normalization is $(4.9 \pm 0.3) \times 10^{-3}$ photons cm^{-2} s^{-1} MeV^{-1}, which yields $\chi^2 = 58/51$ d.o.f. Both normalizations are consistent with each other within the statistical uncertainties.

3.1.3. Joint ROSAT/OSSE spectrum of IC 4329A

We then fitted both simultaneous data sets jointly (with the same model normalization). We used a model consisting of an underlying power law with an exponential cutoff at E_C ($F_E \propto E^{-\alpha}e^{-E/E_C}$) plus reflection, uniform neutral absorption, and an absorption edge. Due to the gap in the data between 2 and 50 keV, the normalization, f_r, of the reflection component is only poorly constrained. Our model reflection spectrum is that of Lightman & White (1988) which calculates the average spectrum seen over all inclinations for an isotropic source illuminating a solar abundance flat slab of material. Then the value of $f_r = 1$ corresponds to an inclination of $\sim 60^o$, while a face on view gives $f_r = 1.33$ (Ghisellini, Haardt & Matt 1994). Uncertainties in geometry lead us to constrain $1 \leq f_r \leq 2$: the *Ginga* data (F92; see below) show the amount of reflection to lie in the middle of this range. The best fit to the OSSE data is then shown by the solid curve in Figure 4a; its parameters are given in Table 2 (model A). We find that a cutoff in the underlying power law is *not* required as the model without a cutoff (dotted curve) gives $\Delta\chi^2 = 2.6$ (for $\alpha = 1.07$ and $f_r = 2$). The relative steepness of the OSSE data can be thus entirely explained by the contribution from the steep high energy component of reflection, without the necessity of an intrinsic spectral break. The EGRET limit implies $E_C \gtrsim 300$ MeV only (for the sum of all EGRET observations).

3.1.4. Joint ROSAT/Ginga/OSSE spectrum of IC 4329A

As discussed above, two past *Ginga* observations have the 2 keV flux identical to that of our *ROSAT* observation. We used those data to construct composite broad-band spectra, which then constrain the spectral parameters much more tightly than the *ROSAT*/OSSE data alone. In particular, they do show the presence of a high energy break in the underlying spectrum. We stress, however, that these composite spectra are less certain than those from *ROSAT*/OSSE alone. In particular, a small change in α from the value seen by *Ginga* can strongly affect the value of E_C.

We have used the *Ginga* data up to 25 keV in our analysis. While including the data above 20 keV might result in a small increase in the overall χ^2 because of the possibility of contamination by the instrumental silver line at 22–25 keV, these data are of relatively low statistical weight. We therefore do not expect this contamination to affect the derived spectral parameters significantly. Nonetheless, to allow for the residual calibration uncertainties, we added in quadrature to the statistical errors a 1% systematic error in the count rate in each PHA channel. Following Piro et al. (1990) and F92, we modeled the data as an absorbed power law with Compton reflection and a Gaussian Fe Kα line. For the observations on 1989 July 8 and 9, we obtained $\alpha = 0.97 \pm 0.06$ and $1.03^{+0.25}_{-0.06}$, $N_{\rm H} = (4.6 \pm 1.3)$ and $(5.0 \pm 1.4) \times 10^{21}$ cm^{-2}, $f_r = 1.06^{+0.41}_{-0.34}$ and 1.33 ± 0.48, the Fe line energy of $E_{\rm Fe} = 6.21 \pm 0.17$ and $6.14^{+0.31}_{-0.39}$ keV, the line flux of $I_{\rm Fe} = (1.34^{+0.50}_{-0.39})$ and $(1.36^{+1.18}_{-0.58}) \times 10^{-4}$ photons s^{-1} cm^{-2} (corresponding to an equivalent width of $\sim$ 135 eV), and χ^2/d.o.f. of 23/28 and 21/28, respectively.

We then fitted the data sets for the three instruments jointly (with the same model normalization). We used the same model as in the *ROSAT*/OSSE fit but now with addition of an iron line. The parameters of the fit are given in Table 2. We have found little difference in the best fit parameters whether using the *Ginga* data of July 8 (model B) or 9 (model C). The total absorbed 0.1–1000 keV X-ray/γ-ray luminosity for model B is 5×10^{44} ergs s^{-1}. As seen from Table 2, the addition of the *Ginga* data constrains α and f_r much more tightly than the *ROSAT*/OSSE data alone. As a consequence, the cutoff energy is also constrained more tightly, between 250 and 1700 keV (models B and C). The model without cutoff (and with reflection) gives $\Delta\chi^2 \simeq 22$ and 8, for models B and C, respectively. Although these model spectra fit the data below 200 keV, they are, however, above the upper limits in the 200–500 keV range. Still, as the *Ginga* observations were not simultaneous with those of *ROSAT* and OSSE, we have to consider the evidence for a high energy break as only tentative. To settle this issue, simultaneous *ASCA* and OSSE (or XTE) observations are necessary.

To aid our understanding of the existence of a cutoff in the spectrum before such observations, we have also used the sum of all the OSSE observations (§§2.2, 3.1.2). OSSE has detected no spectral variability in IC 4329A, which justifies using the average spectrum. Repeating the fits for the OSSE sum we get results given in Table 2, models D, E. There is almost no change in the parameters except that we can constrain E_C even tighter, between 240 and 900 keV. The decreased upper limit on E_C is due to the decreased flux upper limits above 200 keV. Figure 4b shows the spectrum for the model D.

Figure 5 shows the corresponding residuals for the model D. We see that the model is adequate for all three instruments. We get χ^2 per number of PHA channels of 31/47, 22/35, and 55/53, which values are almost identical to those for the best fits for the individual instruments separately.

3.2. Spectrum of the Elliptical Galaxy IC 4329 and the Source S3

The *ROSAT* data for the companion galaxy, IC 4329, were fit in an analogous manner. Here we find that a Raymond & Smith (1976) plasma model (with Solar abundances) fits reasonably well ($\chi^2 = 14/17$ d.o.f.), with a temperature $kT = 0.87 \pm 0.11$ keV, absorbed by a column of $2.8^{+4.0}_{-1.2} \times 10^{20}$ cm^{-2}, entirely consistent with the absorption due to our own Galaxy of 4.55×10^{20} cm^{-2} (measured towards IC 4329A by Elvis, Lockman, & Wilkes 1989, but should not be different by more than a few % within 3′). The corresponding 0.1–2 keV flux is 6.5×10^{-13} ergs cm^{-2} s^{-1}. At $z = 0.0157$, the corresponding luminosity is 6.8×10^{41} ergs s^{-1}, rather average-to-high for its class (Fabbiano, Kim, & Trinchieri 1992). We cannot place any better limits on abundances than $0.2 < A < 3$. We note here that this object was detected with the *Einstein* Observatory HRI (Fabbiano et al. 1992), but that this is the first time its spectral parameters can be measured.

Similarly, we fit the data for the source S3. We find that an absorbed power law, with a column of $3.1^{+2.0}_{-1.7} \times 10^{20}$ cm^{-2} and a spectral index $\alpha = 1.3^{+0.7}_{-0.6}$ fits the data well ($\chi^2 = 8.5/17$ d.o.f); again, the absorption is entirely consistent with the galactic value. The 0.1–2 keV flux is 8.7×10^{-13} ergs cm^{-2} s^{-1}. To the best of our knowledge, this source has not previously appeared as a serendipitous object (e.g., there were no *Einstein Observatory* Imaging Proportional Counter observations of the field of IC 4329A). Judging by its X-ray spectrum and the high galactic latitude, it is likely to be an AGN. However, there are no sources listed in the Veron quasar catalog within 5′ of its X-ray position.

The *ROSAT* spectra and the measured fluxes for both IC 4329 and S3, which over the full *ROSAT* PSPC bandpass are substantially lower than that of IC 4329A, imply that it is unlikely that either object has substantially contaminated the OSSE data, or any previously measured spectra of IC 4329A, obtained with collimated proportional counter instruments as the *Ginga* LAC or *EXOSAT* ME. That is because these instruments are sensitive above 1 keV, where the flux from

IC 4329A dominates by at least a factor of 10. However, around $\sim$ 0.4 keV, the fluxes of all 3 objects are comparable, and below $\sim$ 0.3 keV, IC 4329A is the faintest (see Fig. 6), primarily because its spectrum is more heavily absorbed than the other two sources.

4. CONCLUSIONS

The most important result of this paper is that the spectrum of IC 4329A is compatible with a single power law modified by absorption and reflection extending from soft X-rays to soft γ-rays. The evidence for a spectral break in γ-rays from the simultaneous *ROSAT*/OSSE data is weak, with only a constraint of $E_C \gtrsim 100$ keV. A break between $\sim$ 250 keV and $\sim$ 1700 keV would be required if the simultaneous spectrum in the 2–20 keV range were similar to that from the earlier *Ginga* observations, which have the 2 keV flux in excellent agreement with that seen by *ROSAT*. In any case, the break is at a higher energy than both observed in NGC 4151 ($E_C \sim 50$ keV, Maisack et al. 1993; Zdziarski, Lightman, & Maciołek-Niedźwiecki 1993), and thought before to be typical for Seyfert 1s (F93).

In addition, our *ROSAT* data show that the low energy spectrum is complex, with significantly higher absorption than expected from the column in our own Galaxy. At least a part of this excess absorption ($\sim 3 \times 10^{21}$ cm^{-2}) is likely to be due to cold material, expected from the nearly edge-on orientation of the host galaxy. In addition, there is additional structure in the soft X-ray spectrum, although the modest energy resolution of the PSPC cannot differentiate between an ionized absorber, partial covering by neutral material, or a soft excess.

Further theoretical consequences of this observation are studied in Zdziarski et al. (1994). In that paper, it is shown that the underlying hard X-ray power law can be adequately described by either optically thin ($0.02 \lesssim \tau \lesssim 0.5$) thermal Comptonization, where the scattering medium is mildly relativistic (100 keV $\lesssim kT \lesssim$ 500 keV), or, alternatively, by non-thermal models. In the later case, the lack of a strong (direct or down-scattered) annihilation line in the data requires that electron injection must be at relatively low energies; this can be accomplished when the electron injection is either monoenergetic at a low electron Lorentz factor, $\gamma \sim 3$, or a steep power-law extending down to the minimum $\gamma \lesssim 10$. In all cases, the reflection *is required.* Even though the *Ginga* observations alone allow the "hard tail" to be due to partial covering of the source (but with the column density of $\sim 2.4 \times 10^{24}$ cm^{-2}, about two orders of magnitude greater than would be implied by the spectral structure in the *ROSAT* data), the broad ($\sigma > 0.3$ keV), strong (EW > 100 eV) Fe Kα line (cf. Done 1994) independently implies the presence of the reflecting medium.

This research has been supported in part by the NASA grants NAG5-2439, NAGW-3129 and NAG5-1813, and the Polish KBN grant 221129102. ACF and AC acknowledge the Royal Society and KN acknowledges the SERC for financial support.

APPENDIX : Consideration of the PSPC Instrumental Effects

We considered if it is possible that the edge-like feature is only an artifact of the instrumental effects, and in particular, of miscalibration of the PSPC that would manifest itself as an erroneous resolution matrix. Two such matrices were generated for analysis of the PSPC data : the early version, so-called "92 Mar 11" matrix, and the current version, used in all the analysis above, the "93 Jan 12" matrix. Specifically, we wanted to verify that the fit parameters are only weakly affected by the choice of matrix, and if the confidence regions on the fit parameters overlap. To that end, we prepared a PSPC data set *without* the 2% systematic error added, to make sure that we would not unnecessarily increase the error ranges on the fit parameters (as opposed to the data set used in all previous fitting, which included this 2% error). We then fitted the *ROSAT* data to with both matrices, using the 2 of the models considered in Section 3.1: absorbed power law, and absorbed power law with an edge at $\sim$ 0.7 keV.

The results are summarized in Table 3. It is clear that the improvement in χ^2 is significant regardless of the resolution matrix used, and that the errors on all parameters overlap for fits using both PSPC resolution matrices. We thus conclude that if the differences between the parameters inferred by the use of the two PSPC resolution matrices represent adequately the systematic error in the spectral fits, the parameters of the continuum and the inferred oxygen edge as given in Section 3.1.1 are a good description of the data.

REFERENCES

Done, C., Mulchaey, J. S., Mushotzky, R. F., & Arnaud, K. A. 1992, ApJ, 395, 275
Done, C. 1994, preprint
Elvis, M., Lockman, F. J., & Wilkes, B. J. 1989, AJ, 97, 777
Fabbiano, G., Kim, D.-W., & Trinchieri, G. 1992, ApJS, 80, 531
Fabian, A. C., Nandra, K., Celotti, A., Rees, M. J., Grove, J. E., & Johnson, W. N. 1993, ApJ, 416, L57 (F93)
Fiore, F., Perola, G. C., Matsuoka, M., Yamauchi, M., & Piro, L. 1992, A&A, 262, 37 (F92)
Ghisellini, G., Haardt, F., & Matt, G. 1994, MNRAS, 267, 743
Halpern, J. 1982, Ph. D. Thesis, Harvard University, Cambridge, MA
Kallman, T. & McCray, R. 1982, ApJS, 50, 263
Krolik, J. H., & Kallman, T. 1992, NASA/Goddard preprint
Lightman, A. P., & White, T. R. 1988, ApJ, 335, 57
Maisack, M., et al. 1993, ApJ, 407, L61
Nandra, K., & Pounds, K. 1992, Nature, 359, 215
Nandra, K., & Pounds, K. 1994, MNRAS, 268, 405
Petre, R., Mushotzky, R. F., Krolik, J., & Holt, S. S. 1984, ApJ, 280, 499
Piro, L., Yamauchi, M., & Matsuoka, M. 1990, ApJ, 360, L35
Pounds, K. A., Nandra, K., Stewart, G. C., George, I. M., & Fabian, A. C. 1990, Nature, 344, 132
Raymond, J. C., & Smith, B. H. 1976, ApJS, 35, 419
Wilson, A. S., & Penston, M. V. 1979, ApJ, 232, 389
Yaqoob, T., Warwick, R. S., Makino, F., Otani, C., Sokoloski, J. L., Bond, I. A., & Yamauchi, M. 1993, MNRAS, 262, 435
Zdziarski, A. A., Fabian, A. C., Nandra, K., Celotii, A., Rees, M. J., Done, C., Coppi, P. S., & Madejski, G. M. 1994, MNRAS, in press
Zdziarski, A. A., Lightman, A. P., & Maciołek-Niedźwiecki, A. 1993, ApJ, 414, L93

TABLE 1

PARAMETERS FOR THE ROSAT FITS

Model[1]	N_H[2] (cold)	α	E_{edge} (keV)	τ_{edge}	N_H[2] (ionized[4], or cold partial covering[5])	ξ[3,4] or partial covering fraction[5]	Soft excess (index[6] or blacbody kT [eV][7])	χ^2/d.o.f.
A	2.0 ± 0.3	0.15 ± 0.18	—	—	—	—	—	46.1/44
B	3.0 ± 0.8	0.83 ± 0.4	0.72 ± 0.07	0.56 ± 0.24	—	—	—	30.3/42
C	2.3 ± 0.7	1.0 (fixed)	—	—	$3.8^{+1.4}_{-1.0}$	$3.4^{+22}_{-1.6}$	—	30.4/43
D	$1.8^{+0.6}_{-0.4}$	1.0 (fixed)	—	—	$5.1^{+1.8}_{-0.9}$	$72^{+8}_{-16}\%$	—	32.1/43
E	$5.6^{+1.6}_{-1.1}$	1.0 (fixed)	—	—	—	—	$5.7^{+1.2}_{-0.7}$	32.1/43
F	4.7 ± 0.4	1.0 (fixed)	—	—	—	—	68 ± 10	30.9/43

[1] The models are :
A: Power law with cold absorption;
B: Power law with cold absorption and an edge;
C: Power law with cold absorber plus ionized absorber;
D: Power law with cold absorption plus partial covering by additional cold absorber;
E: Power law with cold absorption plus soft excess (of power law form);
F: Power law with cold absorption plus soft excess (of black body form).
[2] In units of 10^{21} cm^{-2}.
[3] Ionization parameter ξ, as defined in the text.
[4] For Model C.
[5] For Model D.
[6] For Model E.
[7] For Model F.

All errors are given for $\Delta\chi^2 = 2.7$.

TABLE 2

PARAMETERS FOR THE JOINT FITS

Model[1]	N_H[2]	E_{edge}[keV]	τ_{edge}	E_{Fe}[keV]	σ_{Fe}[keV]	I_{Fe}[3]	α	E_C [keV]	f_r	χ^2/d.o.f.
A	$3.0^{+.5}_{-.3}$	.72±.05	$.57^{+.20}_{-.16}$	—	—	—	$.86^{+.21}_{-.13}$	$220^{+\infty}_{-110}$	1^{+1}_{-0}	153/159
B	3.2±.2	.75±.04	$.60^{+.17}_{-.14}$	$6.20^{+.17}_{-.2}$	.33±.33	$1.33^{+.49}_{-.38}$	.94±.03	370^{+270}_{-120}	$1.03^{+.26}_{-.24}$	178/191
C	3.4±.2	.76±.04	.62±.15	$6.10^{+.27}_{-.40}$	$.59^{+.57}_{-.59}$	$1.31^{+.91}_{-.54}$	.98±.04	610^{+1100}_{-270}	$1.17^{+.36}_{-.30}$	181/191
D	3.2±.2	.75±.04	$.60^{+.17}_{-.14}$	$6.20^{+.17}_{-.2}$	$.33^{+.47}_{-.33}$	$1.32^{+.48}_{-.38}$	.93±.03	320^{+150}_{-80}	$1.04^{+.26}_{-.23}$	109/125
E	3.4±.2	.76±.04	$.63^{+.18}_{-.13}$	$6.10^{+.28}_{-.34}$	$.59^{+.57}_{-.59}$	$1.31^{+.90}_{-.53}$	$.98^{+.04}_{-.03}$	480^{+420}_{-160}	$1.18^{+.34}_{-.30}$	113/125

[1] A: simultaneous *ROSAT*/OSSE data only, $1 \leq f_r \leq 2$; B/D and C/E: including *Ginga* data for 1989 July 8 and 9, respectively; D/E: OSSE data for the sum of all observations used;

[2] in units of 10^{21} cm^{-2};

[3] the Fe line flux in units of 10^{-4} photons s^{-1} cm^{-2}.

Errors are given for $\Delta\chi^2 = 2.7$.

TABLE 3

DEPENDENCE OF THE ROSAT SPECTRAL FIT PARAMETERS ON THE ADOPTED PSPC RESOLUTION MATRIX

Model	N_H $\times 10^{21}$ cm^{-2}	α	E_{edge}[keV]	τ_{edge}	χ^2/d.o.f.
CURRENT ("93 JAN 12") PSPC RESOLUTION MATRIX					
Absorbed power law	2.1±0.3	0.16±0.17	—	—	54.2/44
Absorbed power law plus edge	3.0±0.7	$0.84^{+0.41}_{-0.37}$	$0.72^{+0.06}_{-0.07}$	0.56±0.21	34.9/42
"92 MAR 11" PSPC RESOLUTION MATRIX					
Absorbed power law	1.9±0.3	0.19±0.16	—	—	58.6/44
Absorbed power law plus edge	3.4±0.8	1.14±0.45	0.76±0.05	0.62±0.23	37.5/42

Note: See the Appendix for details.

FIGURE CAPTIONS

FIG. 1.—The *ROSAT* PSPC image of the field containing IC 4329A and IC 4329.

FIG. 2.—The *ROSAT* data for IC 4329A, as fitted to a simple, absorbed power law (top) and the resulting residuals (bottom). See Table 1 for the model parameters.

FIG. 3.—The *ROSAT* data for IC 4329A, as fitted to an absorbed power law with an edge at 0.72 keV (top) and the resulting residuals (bottom). See Table 1 for the model parameters.

FIG. 4.—The broad-band spectrum (in EF_E) of IC 4329A. The crosses give the data, the solid curves represent the best fit power law with an exponential cutoff, reflection, Fe K line, and absorption (see Table 1, models A, D, for parameters); the dashed curves represent the power law component with the cutoff but without the contribution from reflection. It is apparent that the reflection contribution is important in the OSSE energy range. For comparison, the dotted curves show the best-fit spectrum for the model without the cutoff. The upper limits are 2-σ. (a) The *ROSAT* (< 2 keV) and OSSE (> 50 keV) data. One sees that both models with and without the exponential cutoff are compatible with the data, which is possible due to a change in the spectral index (see Table 1). (b) The data including the non-simultaneous *Ginga* data (2–25 keV) and the sum of all OSSE observations of IC 4329A. The model without the cutoff is ruled out as the spectral index is fixed by the *Ginga* data.

FIG. 5.—The unbinned residua of the best fit shown in Fig. 1b, for *ROSAT*, *Ginga*, and OSSE, from bottom to top, respectively. It is apparent that the agreement of the raw data with the model is excellent. The lack of significant residuals above 200 keV (where no signal is detected) shows the level of accuracy of the background subtraction.

FIG. 6.—The best-fitting spectral models for the 3 brightest sources (IC 4329A, IC 4329, and S3) present in the *ROSAT* field of view. While IC 4329A is by far the strongest source above 0.5 keV, the other two sources, if not spatially resolved, could provide significant flux contamination below 0.3 keV.

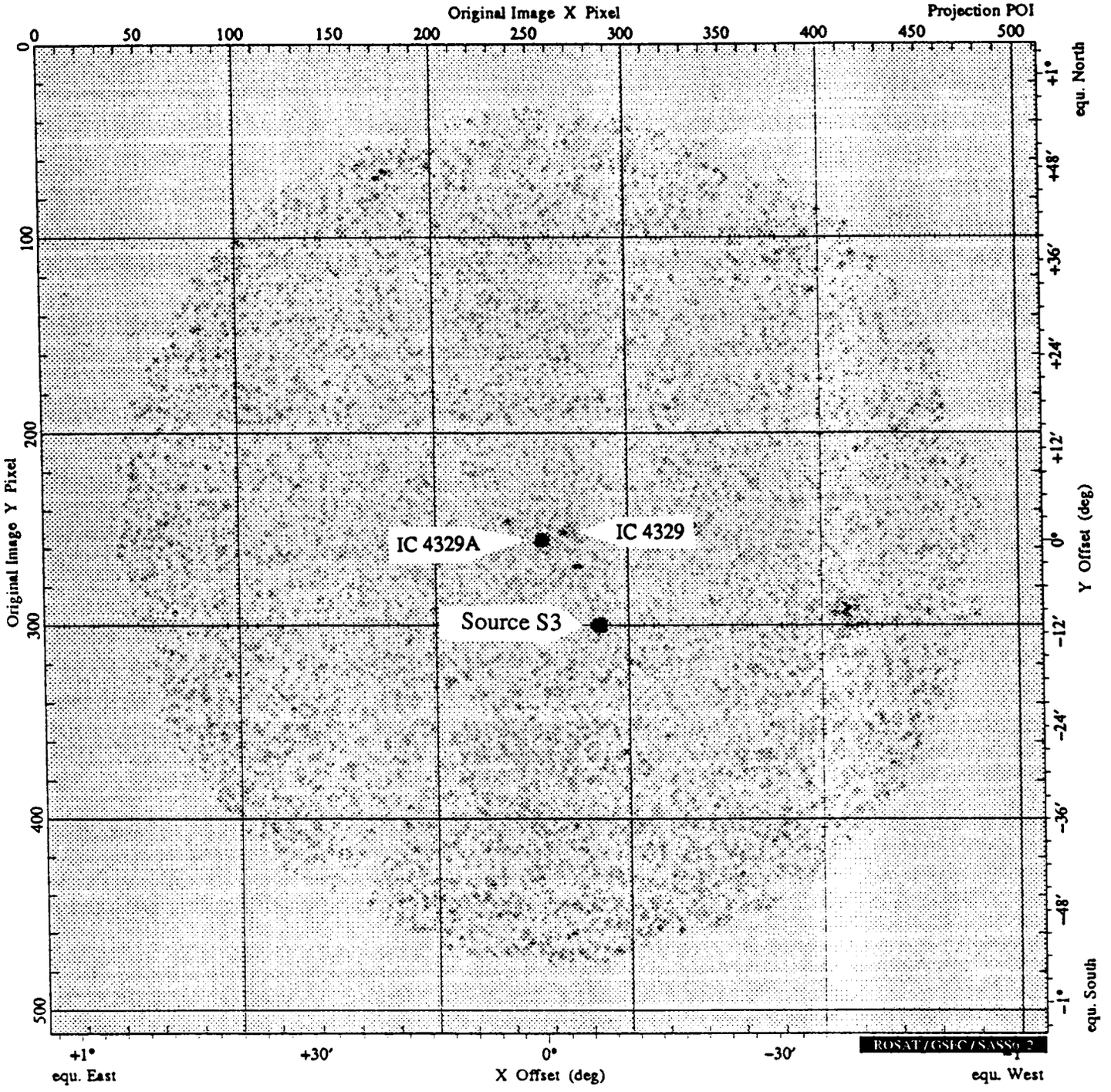
Original Image X Pixel
Projection POI
0
50
100
150
200
250
300
350
400
450
500
Original Image Y Pixel
100
200
300
400
500
IC 4329A
IC 4329
Source S3
+1°
+30′
0°
-30′
-1°
equ. East
X Offset (deg)
equ. West
equ. North
+48′
+36′
+24′
+12′
0°
-12′
-24′
-36′
-48′
equ. South
Y Offset (deg)
ROSAT/GSFC/SASS

Figure 1

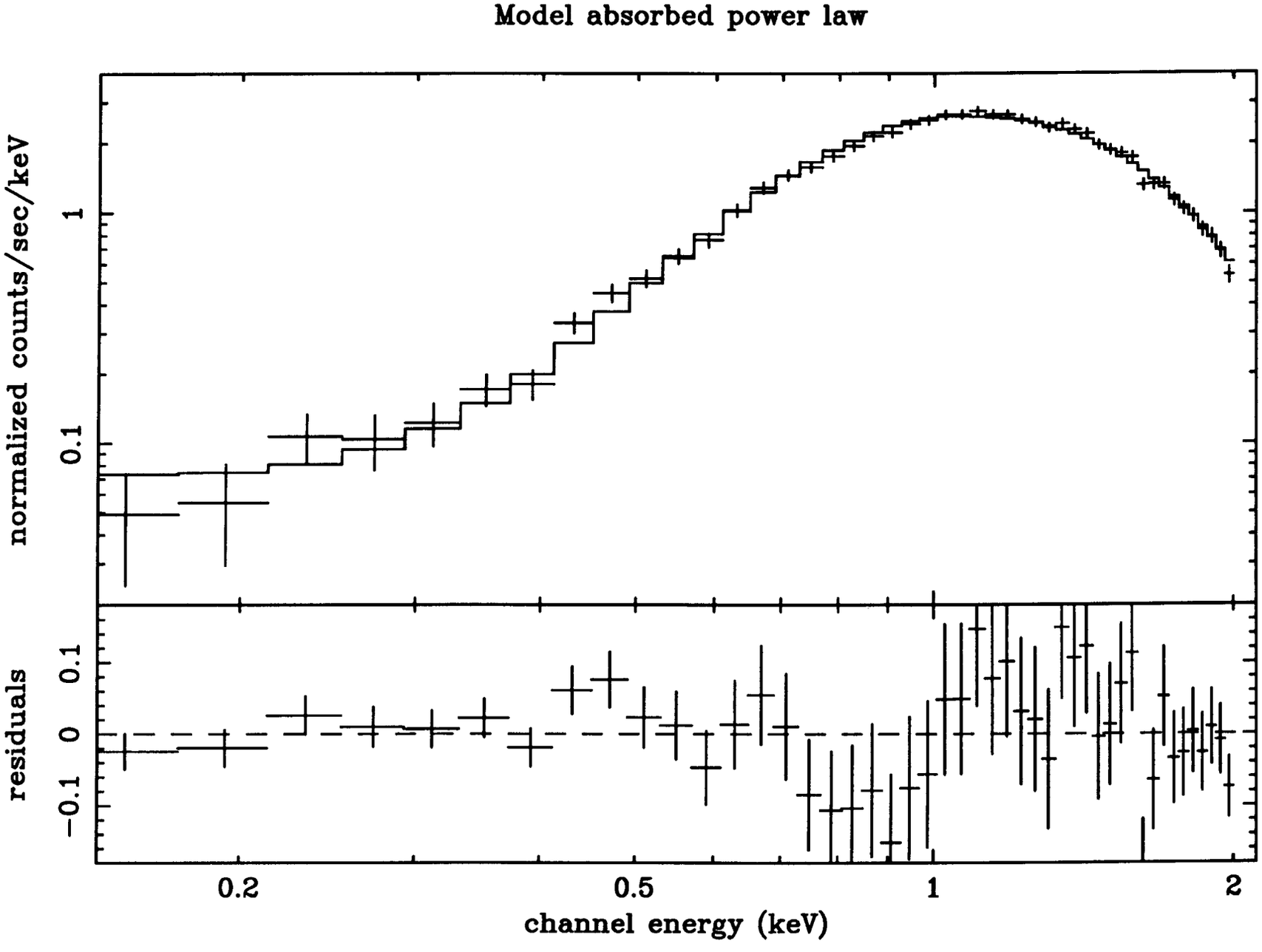
Model absorbed power law
normalized counts/sec/keV
1
0.1
residuals
0.1
0
−0.1
0.2
0.5
1
2
channel energy (keV)

Figure 2

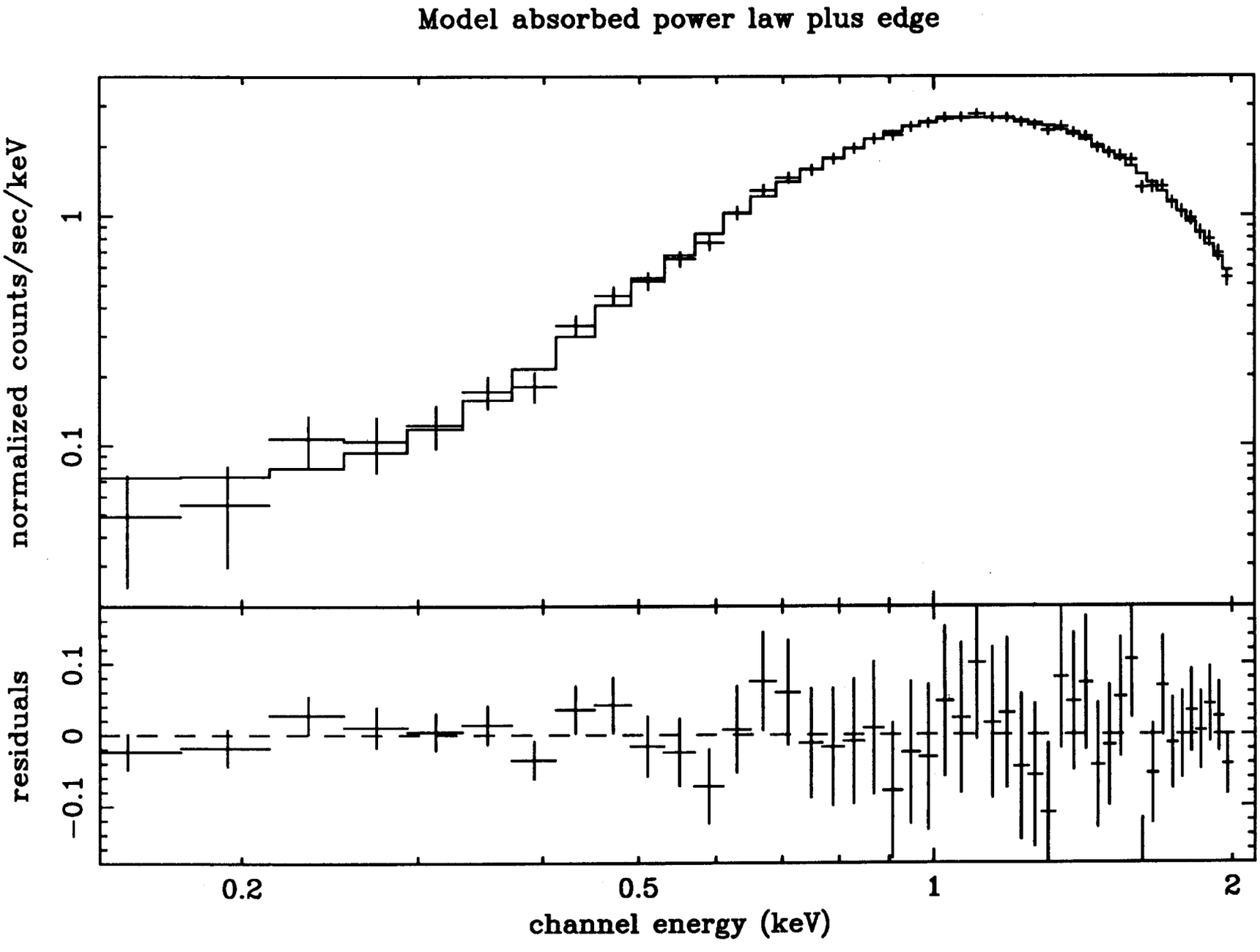
Model absorbed power law plus edge
normalized counts/sec/keV
1
0.1
residuals
0.1
0
−0.1
0.2
0.5
1
2
channel energy (keV)

Figure 3

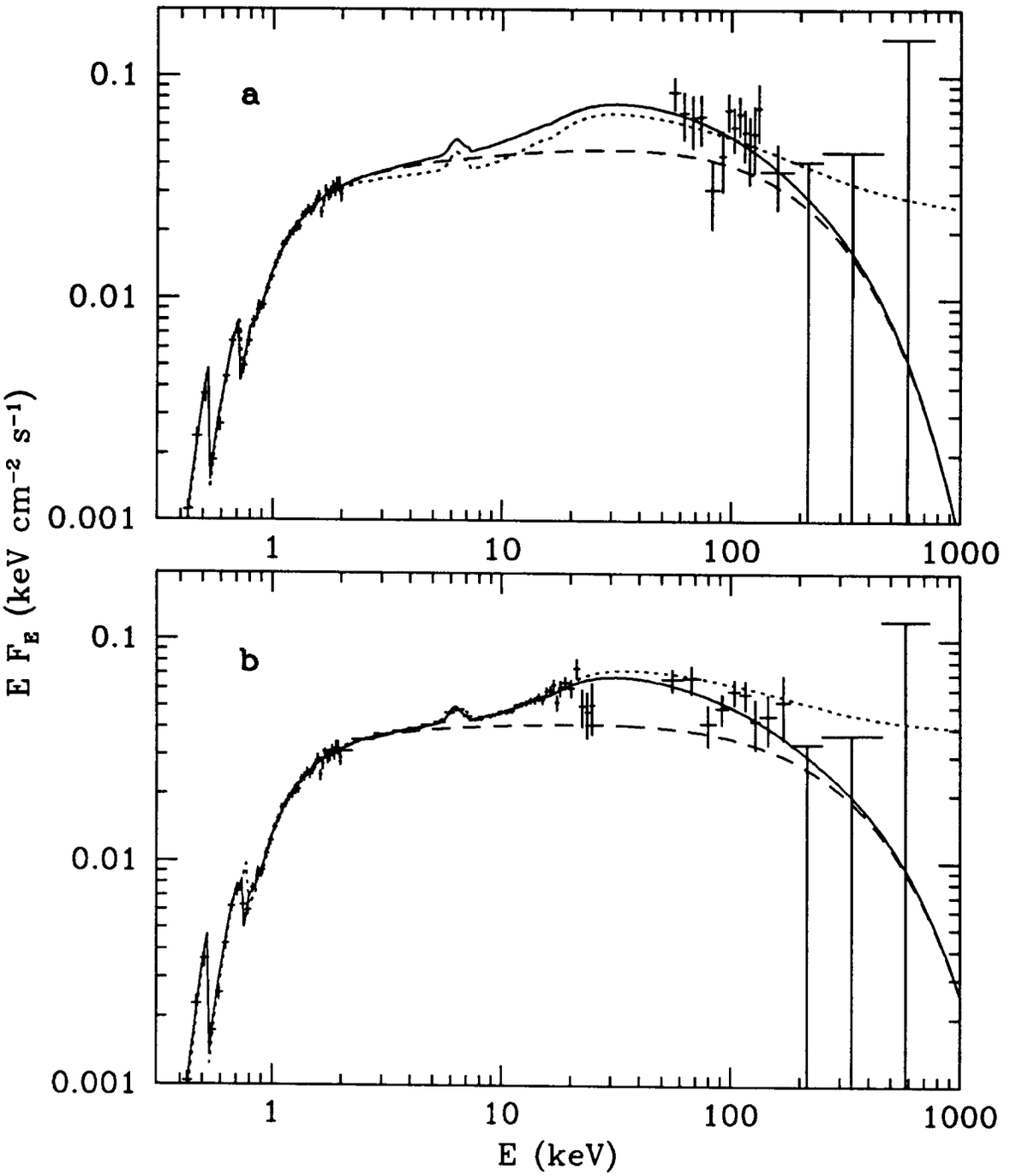

Figure 4

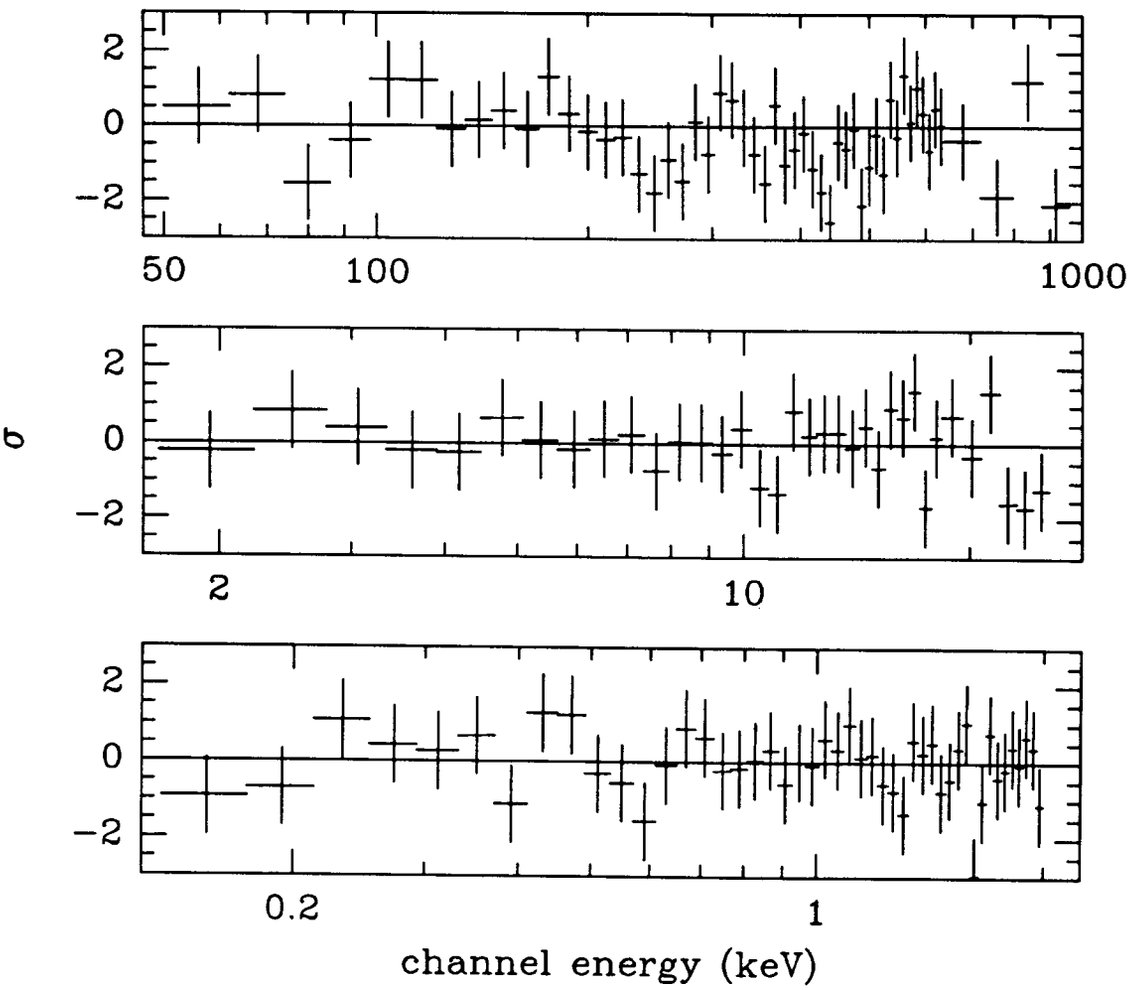

Figure 5

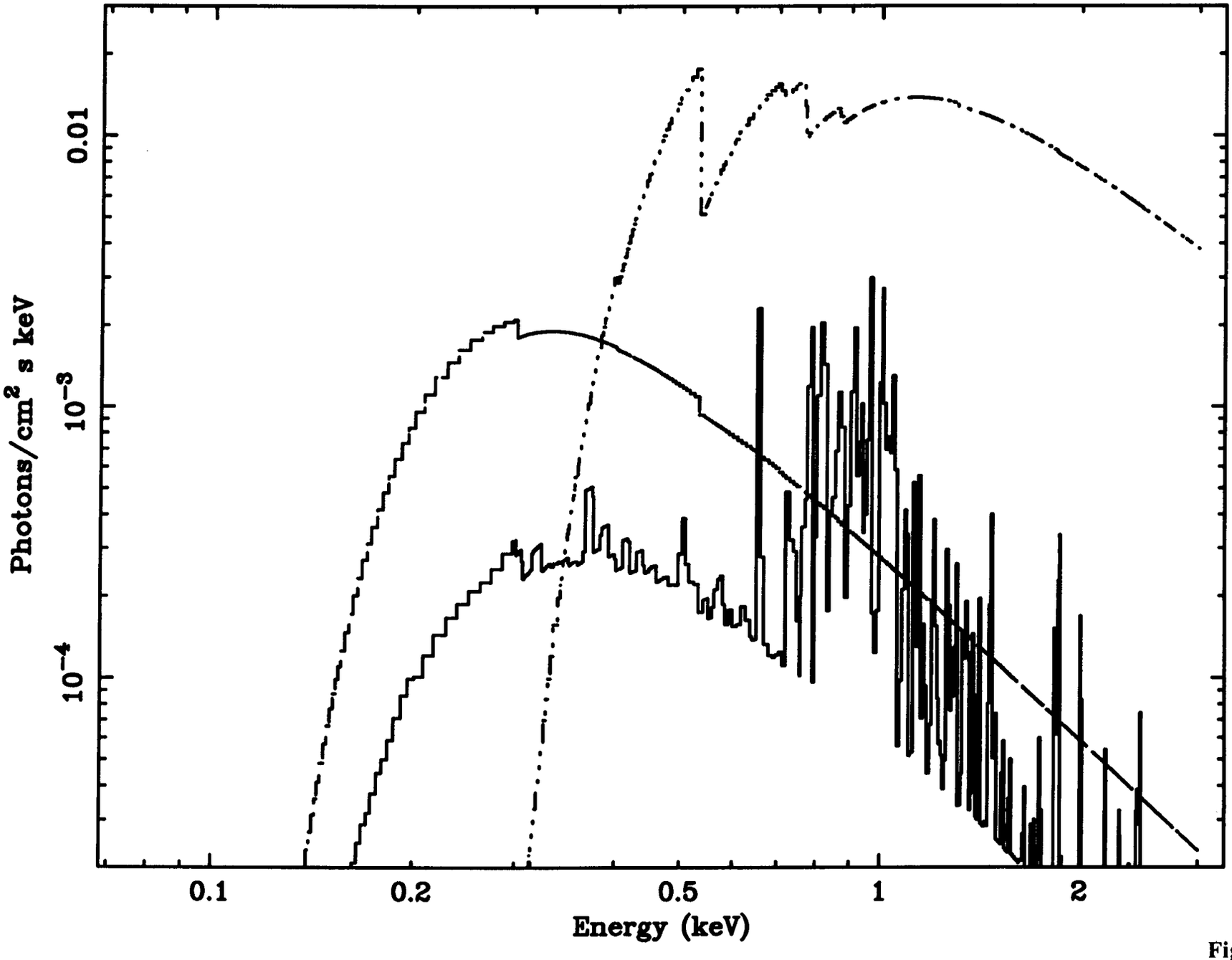

Figure 6

Mon. Not. R. Astron. Soc. 000, 000–000 (1994)

Physical processes in the X-ray/gamma-ray source of IC 4329A

A. A. Zdziarski[1], A. C. Fabian[2], K. Nandra[2], A. Celotti[2], M. J. Rees[2], C. Done[3], P. S. Coppi[4], and G. M. Madejski[5,6]
[1] *N. Copernicus Astronomical Center, Bartycka 18, 00-716 Warsaw, Poland; e-mail: aaz@camk.edu.pl*
[2] *Institute of Astronomy, Cambridge, UK*
[3] *Physics Dept., Leicester University, UK*
[4] *Dept. of Astron. and Astrophys., Univ. of Chicago, 5640 Ellis Ave., Chicago, IL 60637, USA*
[5] *Lab for High Energy Astrophysics, NASA/Goddard, Greenbelt, MD 20771, USA*
[6] *Universities Space Research Association, USA*

20 June 1994

ABSTRACT
Theoretical implications of the recent simultaneous *ROSAT*/OSSE observation of the Seyfert 1 IC 4329A are discussed. We find that either thermal or nonthermal Comptonization models can fit the data. Thermal models require optically-thin plasma and mildly relativistic electrons. Nonthermal models require most of the injected power to be at low values of the electron Lorentz factor. Both models predict a spectral cutoff at energies below ~1 MeV, which agrees with broad-band data including non-simultaneous *Ginga* spectra that match the *ROSAT* 2 keV flux. Also, Compton reflection corresponding to cold matter covering a 2π solid angle is required, and partial covering is ruled out.
Since the spectrum of IC 4329A is typical of Seyfert 1s, their contribution to the cosmic hard X-ray background can be estimated; without cosmological evolution, it is 30% at 3 keV. However, as the peak of the νF_ν spectrum of IC 4329A is much broader than that of the hard X-ray background, Seyfert 1s cannot account for the X-ray background spectrum without spectral evolution.

Key words: Galaxies: individual: IC 4329A – Galaxies: Seyfert – X-rays: galaxies – diffuse radiation – plasmas – gamma-rays: theory

1 INTRODUCTION

In this paper, we discuss theoretical implications of the simultaneous observation of the Seyfert 1 IC 4329A by *ROSAT* and OSSE aboard *GRO* (Madejski et al. 1994, hereafter M94). The data in M94 are well-fitted by an intrinsic power law with an exponential cutoff, external absorption, and a Compton reflection component (using the angle-averaged formulae of Lightman & White 1988 and White, Lightman, & Zdziarski 1988). The best fit parameters are: the power law energy index of $\alpha = 0.86^{+0.21}_{-0.13}$, the cutoff energy of $E_C = 220^{+\infty}_{-110}$ keV, and the (poorly constrained) relative normalization of the reflected component (f_r) of about unity (model A in M94). An exponential cutoff is not required by the *ROSAT*/OSSE data; only the upper limit by *GRO* EGRET implies that $E_C \lesssim 300$ MeV. The model with $E_C = 300$ MeV has $\alpha = 1.07$ and $f_r = 2$.

The spectral constraints become much tighter with the inclusion of archival *Ginga* data. Although these are not simultaneous they match the flux measured by *ROSAT* at 2 keV. The best fits to two sets of *Ginga* observations give $0.91 < \alpha < 1.02$, 250 keV $< E_C <$ 1700 keV, and $0.8 < f_r < 2.2$ (models B, C in M94). As the X-ray spectral *shape* in IC 4329A is fairly constant (Fiore et al. 1992), these parameters give indeed a plausible broad-band spectrum of the AGN. Furthermore, M94 find that the OSSE spectrum also remains constant with time, which allows them to use the spectrum from the sum of this and 2 previous OSSE observations. This reduces the allowed range of E_C to between 240 and 900 keV. We note that this E_C is much larger than that seen in the brightest Seyfert, NGC 4151 (Maisack et al. 1993; Zdziarski, Lightman, & Maciołek-Niedźwiecki 1993).

The X-ray and γ-ray spectrum of IC4329A is very typical for Seyfert 1s. Its intrinsic X-ray spectral index is consistent with the average one for Seyfert 1s, $\alpha = 0.95 \pm 0.05$ (Pounds et al 1990; Nandra & Pounds 1994, hereafter NP94), and with a relative normalization of the reflection component close to the average Seyfert value ($f_r \simeq 1.0 \pm 0.2$, NP94; note that we have multiplied their normalization, corresponding to the face-on reflection spectrum, by 1.33 in order to get f_r for the angle-averaged reflection spectrum; see

Ghisellini, Haardt, & Matt 1994). The γ-ray spectral index in the OSSE range (50–200 keV), $\alpha = 1.6 \pm 0.2$, is again very similar to the average index for Seyferts observed by OSSE, $\alpha = 1.4 \pm 0.25$ (Johnson et al. 1994). Thus, unlike NGC4151, conclusions regarding the nature of the X-ray/γ-ray source in IC 4329A are likely to be applicable to Seyfert 1s as a class. In particular, the contribution of Seyfert 1s to the cosmic X-ray background (hereafter XRB) can be re-evaluated using the spectrum of IC4329A.

2 MODELS OF THE X-RAY/γ-RAY SOURCE

2.1 Thermal Compton Scattering

Optically thin thermal Compton scattering spectra are well represented by power laws with exponential cutoffs (e.g., Zdziarski 1986). This spectral form was in fact used to fit the data (§1, M94). An intrinsic spectrum with $\alpha = 0.95$ and $E_C = 400$ keV (within the confidence regions of models D, E in M94) is almost identical to the thermal Comptonization spectrum (obtained using the Monte Carlo method of Górecki & Wilczewski 1984) from a slab irradiated from below by UV photons with $kT = 256$ keV ($E_C \simeq 1.6kT$) and $\tau = 0.09$, as shown on Figure 1. The scattering plasma has to be *optically thin* in general, since the allowed range of $\alpha \simeq 1$ and E_C (> 110 keV, using the *ROSAT*/OSSE data only, M94) implies $\tau \lesssim 0.5$ (see eqs. [1]-[2] below). Compton scattering in optically thick plasmas (Sunyaev & Titarchuk 1980) is ruled out.

Quantitatively, for optically thin plasmas we have,

$$\alpha \simeq \frac{-\ln P}{\ln(1 + 4\Theta + 16\Theta^2)} \qquad (1)$$

(Zdziarski 1985, hereafter Z85; Pozdnyakov, Sobol', & Sunyaev 1977), where $\Theta \equiv kT/m_e c^2$, and P is the average scattering probability, which for a uniform slab is,

$$P = 1 + \frac{\exp(-\tau)}{2}\left(\frac{1}{\tau} - 1\right) - \frac{1}{2\tau} + \frac{\tau}{2}E_1(\tau) \qquad (2)$$

$$\rightarrow \begin{cases} -(\tau/2)\ln\tau, & \tau \ll 1; \\ 1 - 1/(2\tau), & \tau \gg 1, \end{cases}$$

where E_1 is the exponential integral (Press et al. 1992). Equations (1)-(2) fit Monte Carlo results well for any T, for $\tau \lesssim$ a few.

Furthermore, Monte Carlo simulations show that spectra for $\Theta \gtrsim 1$ (which correspond to $\tau \lesssim 0.02$ and $E_C \gtrsim 800$ keV) are very bumpy with distinct individual scattering profiles (see, e.g., Haardt & Maraschi 1993, hereafter HM93). Since the intrinsic X-ray power law in IC 4329A is smooth, $E_C \lesssim 800$ keV is required, which approximately agrees with the fitted maximum E_C, models D, E, M94 (unless a spatial distribution of plasma parameters is fine-tuned to give a smooth $\alpha \simeq 1$ power law over the 1–30 keV range).

The parameters for the thermal Comptonization model in Figure 1 are consistent with the disk-corona model of HM93 with most of the accretion power released in the corona. This is because in our Monte Carlo model the seed photon power equals almost exactly the power in the photons scattered back towards the slab (crosses in Fig. 1) and thermalized. This then implies that all the disk thermal emission is due to reprocessing of the hard X-ray flux, and that the intrinsic, thermal, viscous stress emission from the disk is negligible. Models with $E_C \lesssim 400$ keV require larger τ in order to produce the observed α. For the same incident blackbody flux, the scattered spectrum (which starts at a point a factor of $\sim \tau$ below the peak flux of the blackbody) is then higher in normalization. Thus these models predict rather more reprocessed blackbody flux than for $E_C = 400$ keV and so is not consistent with the disk corona model. However, this problem can be circumvented if a fraction of the reprocessed photons do not return to the hot scattering cloud (which can be achieved if the hot cloud is at some height above the disk). On the other hand, models with $E_C \gtrsim 400$ keV allow for some dissipation taking place in the disk.

Is the X-ray/γ-ray source made of electrons or of pairs? As the plasma is optically thin, the answer depends sensitively on the pair escape rate (Z85). In the absence of that process, the "standard" pair equilibrium (e.g., Svensson 1984) applies, with the pair production rate (dominated by photon-photon interactions) balanced by pair annihilation in the hot cloud. The plasma is pair-dominated for the maximum allowed (local) compactness, $\ell_l \sim 20$ for $E_C = 400$ keV, which decreases (increases) quickly with the increasing (decreasing) E_C (see Fig. 3b in HM93). The annihilation feature is, however, broad and not distinguishable from the continuum (Zdziarski 1986). For ℓ_l much lower than

Figure 1. An optically thin thermal Comptonization model for the intrinsic spectrum of IC 4329A. Blackbody photons (dashed curve; $kT_{\rm bb} = 10$ eV) emitted by a disk are Compton upscattered in a thermal corona with $kT = 256$ keV and $\tau = 0.09$. Circles and crosses give the spectrum of photons emitted away and of photons scattered back to the disk, respectively. The power in those spectra is 1.0 and 1.25, respectively, of the power in the seed photons. Note that the total emitted spectrum also includes unscattered blackbody photons (not shown here). The solid curve, which gives the intrinsic spectrum of IC 4329A [$\propto E^{1-\alpha}\exp(-E/E_C)$, $\alpha = 0.95$, $E_C = 400$ keV], approximates well the emitted spectrum. As $\sim 80\%$ of the power in photons scattered back to the disk is absorbed and thermalized ($\sim 20\%$ is reflected by the cold disk, which component is not shown here), all the blackbody emission is due to the absorbed power and very little internal dissipation in the disk is allowed. Thus, this model fits well the dissipative corona/disk scenario of HM93.

the maximum $\ell_l(E_C)$, the plasma is e^--dominated. Furthermore, in the corona geometry we have to distinguish the local compactness, i.e., one corresponding to the luminosity produced locally in a volume with the size equal to the corona scale height, H, from the global compactness, $\ell \equiv L\sigma_T/(Rm_ec^3) \simeq (3R/H)\ell_l$, where R is the corona radius (Björnsson & Svensson 1991). In gas-pressure dominated e^- coronae, $H/R \simeq 0.03r^{1/2}$, where $r \equiv R/R_S$ (Svensson & Zdziarski 1994), and thus $\ell \simeq 100r^{-1/2}\ell_l$. From the observed iron line width, $r < 50$ (Done 1994), and thus the corona would be e^--dominated for $\ell \ll 300$ (at $E_C = 400$ keV).

However, pair escape can cause the corona to be e^--dominated even at much larger ℓ. Pairs can diffuse to the disk with an effective pair velocity β and annihilate there or be blown away by the radiation pressure. (Note that an annihilation line from escaping pairs is negligibly weak, with the local compactness in the annihilation photons of $< \beta\tau \ll 1$.) The ratio of this process to the coronal annihilation is $\sim 20\beta/\tau \sim 200\beta$ (at $\Theta = 0.5$, Z85). The compactness at which the corona can be pair-dominated increases then by the same factor and the condition for the e^--domination in the paragraph above becomes $\ell \ll 6 \times 10^4\beta$. Since $\ell < 10^3$ is expected in sub-Eddington accretion sources (Svensson 1987, hereafter S87), any $\beta \gtrsim 0.02$ (i.e., even much below the sound speed) would cause the corona to be e^--dominated. Concluding, the corona in IC 4329A is likely to consist of electrons unless pair escape to both the disk and the exterior is strongly suppressed.

2.2 Nonthermal Plasmas

As discussed in §1, a spectral break in the intrinsic (power law) spectrum is *not* required if one takes into account only the simultaneous *ROSAT*/OSSE data. A single power-law spectrum extending to γ-rays can be naturally produced by nonthermal power law electrons with the power law index of $p = 2\alpha + 1 \simeq 3$ (e.g., Blumenthal & Gould 1970). The power law electrons can scatter, e.g., UV photons emitted by an accretion disk. If this is the case, the power law distribution has to continue down to the Lorentz factors $\gamma \sim 3$, for the upscattering of the UV photons (with characteristic energy of ~ 50 eV or so) to form a power law with $\alpha \simeq 1$ above 0.7 keV, as required by the data (M94). Also, the compactness of the nonthermal source has to be low, $\ell_{\rm nth} \lesssim 1$, for pair production not to modify the power law spectrum (e.g., S87; Lightman & Zdziarski 1987). In this limit, pair absorption cuts off the spectrum above $E_C \sim 150\,{\rm MeV}/\ell_{\rm nth}$ (S87).

However, the compactness in accreting black hole sources is likely to be $\gtrsim 1$ (S87) and then the pair production effects dominate. The energetic electrons cool before they can escape, so their distribution is described by the continuity equation where the injected spectrum is balanced against Compton cooling. For injected distributions of the form γ^{-s}, $s < 1$ gives $p = 2$, while for $s \geq 1$, $p = s + 1$. "Standard" nonthermal pair models use monoenergetic injection of pairs or electrons, which Compton cool on the UV photons to produce a power law particle distribution of $p = 2$ (e.g., S87). Thus, for $\ell_{\rm nth} \ll 1$ the spectrum has $\alpha = 0.5$. Increasing $\ell_{\rm nth}$ increases the amount of pair reprocessing if γ-rays are produced, i.e., for large particle Lorentz factors. This increases the spectral index to $\alpha \sim 1$, but also increases the numbers of cooled pairs in the source. This gives rise to a pair annihilation line containing about 10% (the pair yield) of the injected power. Downscattering of the line superimposed on the nonthermal emission and the reflection component causes the spectrum above ~ 200 keV to be *above* the observational upper limits. The best-fit monoenergetic injection pair model of Lightman & Zdziarski (1987, fitted to the same data set as in model D of M94) has $\ell_{\rm nth} = 70 \pm 20$ with the injection at $\gamma_i = 6000^{+4000}_{-1500}$, the compactness corresponding to the seed blackbody photons (at $kT_{\rm bb} = 10$ eV), $\ell_{\rm bb} = 600$, and the reflection normalization, $f_r = 1.0 \pm 0.2$. The model yields $\Delta\chi^2 = 25$ with respect to the best fit thermal model (D in M94), which increase is due mostly to the photon flux in the 180–360 keV range being 4-σ above the OSSE sensitivity. The fit can be only slightly improved if one allows for pair escape (either diffusion to the disk or pair wind, see §2.1) since this gives fewer cooled pairs and a weaker annihilation feature. For the effective escape velocity $\beta = 0.3$, $\Delta\chi^2 = 17$, which still allows us we rule out the monoenergetic injection nonthermal model.

Figure 2. A fit of a nonthermal model with $e^\pm$ pair production and a power law pair injection to the broad-band spectrum of IC 4329A (from *ROSAT*, *Ginga*, and OSSE; the upper limits are 2-σ). The dashed curve gives the nonthermal pair emission alone, and the solid curve is the sum of the pair emission and a Compton reflection component (with an iron Kα line). The parameters are: $s = 2.8 \pm 0.4$, $\ell_{\rm nth} = 70 \pm 50$, $\gamma_{\rm min} = 5$, $\gamma_{\rm max} = 10^3$ (fixed), $\ell_{\rm bb} = 30 \pm 20$, and $f_r = 1.50 \pm 0.19$.

On the other hand, nonthermal models with substantial power supplied to the source at moderately relativistic energies have lower pair yield and can fit the data. One example is a model with a steep power-law injection (which gives a steep intrinsic spectrum, which produces fewer secondary pairs). The best-fit model (Ligthman & Zdziarski 1987; fitted to the same data set as in model E of M94) is shown in Figure 2. It yields the same χ^2 as the best-fit thermal model. Still, the model predicts the photon flux in the 180–360 keV range at 2.8-σ above the OSSE sensitivity. Since this sensitivity can be reduced by increasing the detection time, this model can be tested in the near future.

As noted by, e.g., Ghisellini, Haardt, & Fabian (1993), electron injection at a $\gamma_i \lesssim 5$ gives rise to spectra extending only slightly above the threshold for pair production, which results in very few pairs. The spectra in this model are from repeated Compton scattering by nonthermal electrons and are very similar to those from thermal Compton scattering.

We have tested this model using the code by Coppi (1992) and obtained a good fit ($\alpha \simeq 1$ and a strong cutoff above $\sim$ 300 keV) for $\ell_{\rm nth} = 70$, $\ell_{\rm bb} = 20$, and monoenergetic electron injection at $\gamma_{\rm i} = 3.5$.

2.3 The Presence and State of Reflecting Medium

Can the spectrum of IC 4329A be explained by partial covering rather than reflection? The *continuum* spectral signature of reflection is quite similar to that of partial covering by substantial column density ($\sim 10^{24}$ cm^{-2}) of cold material (Piro, Yamauchi & Matsuoka 1990). The absorbed spectrum only contributes above $\sim$ 10 keV, so the sum of it with the direct component produces a high energy excess. Note that this is very different from the partial covering considered in M94, where much lower N_H ($\sim 5 \times 10^{21}$ cm^{-2}) was used to account for the observed excess below 0.7 keV. However, partial covering, unlike reflection, has the same shape at high energies as the incident spectrum, so a break at an energy lower than in the reflection model is required, as reflection no longer contributes to the steepening in the OSSE band. An incident power law spectrum without a break or cutoff is now ruled out at higher significance than in the case of reflection ($\chi^2 = 172/127$ d.o.f., fitted to the data as in model D of M94). The intrinsic steepening in the *ROSAT*/*Ginga*/OSSE data can be modelled either by an exponential cutoff power law spectrum [$\alpha = 0.85 \pm 0.03$, $E_C = 170^{+60}_{-40}$ keV, $N_H = (2.4 \pm 0.7) \times 10^{24}$ cm^{-2} and covering fraction 0.29 ± 0.05, $\chi^2 = 105/124$ d.o.f.] or by a broken power law ($\alpha_1 = 0.88 \pm 0.02$, $\alpha_2 = 2.7 \pm 0.3$, $E_{\rm break} = 55 \pm 19$ keV, $\chi^2 = 109/123$ d.o.f) with similar partial covering parameters.

However, it is difficult to reproduce the observed line emission from such models. For the fitted partial covering, the line equivalent width would be only $\sim$ 30 eV (Inoue 1989) whereas the observed equivalent width is about 130 eV (M94), which agrees with the reflection model (George & Fabian 1990). External sources of the line may be important (Ghisellini et al. 1994) but in that case, a line much narrower than observed ($\sigma_{\rm Fe} \sim 0.5$ keV, Done 1994) would be produced. Thus, we can rule out partial covering as a model for the overall X-ray/γ-ray spectrum.

The reflecting medium is likely to be partially ionised by the incident photons. We have fit ionised reflection spectra (Done et al. 1990) to the *ROSAT*/*Ginga* spectra and found that $\xi \equiv L/n_e R^2 \lesssim 50$, where L is defined as the total ionising luminosity between 5 eV and 300 keV. Over the more usual bandpass of 13.6 eV–13.6 keV this corresponds to $\xi \lesssim 30$, where iron is less ionised than FeXV. This is rather smaller than the ionisation required to produce the observed soft X-ray excesses in some Seyferts from reflection alone (Czerny & Życki 1994).

3 CONTRIBUTION TO THE X-RAY/γ-RAY BACKGROUND

As discussed in §1, the spectrum of IC 4329A is typical for Seyfert 1s. We thus use it to estimate the contribution of Seyfert 1s to the XRB. The volume emissivity at $z = 0$ from local sources is estimated to be $\sim 10^{39} h$ ergs s^{-1} Mpc^{-3} [$h \equiv H_0/(100$ km s^{-1} Mpc^{-1})] in the 2–10 keV range (Lahav et al. 1993), which is in fact the same as the estimated local AGN emissivity, dominated by Seyferts (Piccinotti et al. 1982). The solid curve in Figure 3 shows the contribution to the XRB assuming the best-fit spectrum of IC 4329A (model D in M94) and no evolution up to $z_{\rm max} = 5$. The Seyfert 1 contribution to the XRB is then about 30% at 3 keV and 18% at 30 keV.

On the other hand, Seyfert 1s may undergo evolution of the comoving volume emissivity. We find it has to be slower than $(1+z)^\beta$, $\beta \simeq 1.6$ (with no spectral evolution and $\Omega_0 = 0$) as the case with $\beta = 1.6$ already produce most of the 2 keV XRB (dotted curve in Fig. 3). However, the integrated Seyfert 1 spectrum peaks at a too low energy (20 keV) and is much too soft at low energies to possibly explain the XRB peak at 30 keV. This is just a manifestation of the well-known spectral paradox (Boldt 1987), the striking difference between the spectra of the XRB and of observed AGNs. To reproduce the hard XRB, either suitable *spectral* evolution or a new class of sources is required.

It turns out that the contribution of Seyfert 1s to the background cannot constrain the exponential cutoff energy in the spectra of individual Seyfert 1s. The dashed curve shows the source model with $\alpha = 1.07$ and the high $E_C = 300$ MeV (see §1), and without evolution. We see that this contribution is entirely within the measured γ-ray background. This conclusion differs from one in Rothschild et al. (1983), who required a break in the Seyfert 1 spectrum based on the contribution to the γ-ray background. The difference is due to their average Seyfert 1 spectrum with $\alpha = 0.7$, whereas *Ginga* showed the intrinsic Seyfert 1 power law index to be $\alpha \simeq 1$ (NP94).

4 CONCLUSIONS

The simplest description of the spectrum of IC 4329A is in terms of thermal Comptonization. In this model, the scattering medium has to be *optically thin*, with the Thomson optical depth $0.02 \lesssim \tau \lesssim 0.5$, and mildly relativistic, 100 keV $\lesssim kT \lesssim 500$ keV. Optically thick Comptonization (Sunyaev & Titarchuk 1980) is ruled out. The best fit parameters, $\tau \simeq 0.1$ and $kT \simeq 250$ keV, fit well the dissipative disk-corona model of HM93. The plasma in the corona is most likely electron-dominated.

The spectrum can also be fitted by nonthermal models, with either power-law electron injection extending to $\gamma \ll 10$ (and pair production), or monoenergetic injection at $\gamma_{\rm i} \sim 3$, for which very few pairs are produced. Nonthermal pair models with monoenergetic injection (at $\gamma_{\rm i} \gg 10$) and pair production are ruled out as they strongly over-predict the flux above 180 keV. This excess flux is partly due to Compton downscattering of the annihilation line.

Both classes of models require a substantial contribution from Compton reflection, and partial covering by optically thick matter is ruled out. The high-energy tail of reflection is important in the OSSE range, resulting in the incident spectrum being harder than the observed one. Therefore, the break energy in the incident spectrum is at much larger energy ($\sim$ 500 keV) than the break in the observed spectrum (at $\sim$ 30 keV). Since the spectrum of IC 4329A is very typical for Seyfert 1s, this conclusion is likely to ap-

Figure 3. The possible contributions of Seyfert 1 galaxies with the IC 4329A-like spectrum to the cosmic X-ray and γ-ray background. The 0.5–2 keV error contour gives the preliminary *ROSAT* results (Hasinger 1992); circles are a compilation of best results from various experiments by Gruber (1992); the dashed region is the systematic error contour for the *Apollo* results, with the middle dot-dashed curve being the best estimate of the spectrum (Trombka et al. 1977); and the 35–100 MeV error contour is from Fichtel et al. (1978). The models are for $\Omega_0 = 0$, and the 2–10 keV local emissivity of $10^{39}h$ ergs s^{-1} Mpc^{-3}. The solid and dashed curves give the case without evolution for $z_{\max} = 5$ and for $\alpha = 0.93$, $E_C = 320$ keV, $f_r = 1.04$, and $\alpha = 1.07$, $E_C = 300$ MeV, $f_r = 2$ (M94), respectively. The dotted curve corresponds to the fastest allowed evolution ($\beta = 1.6$, $z_{\max} = 4$) for the model with $E_C = 320$ keV.

ply to the average Seyfert 1 spectrum, for which a break at $\sim$ 50 keV was inferred based on models *without* reflection (Johnson et al. 1994).

The contribution of Seyfert 1s to the hard XRB based on the IC 4329A spectrum is about 20–30% without evolution. The contribution fits neither the 3–10 keV slope nor the 30 keV peak in the background. To fit the XRB, spectral evolution or a different class of objects is required.

ACKNOWLEDGMENTS

This research has been supported in part by the NASA grants NAG5-1813, 2439, NAGW-830, 1284, 1636, 3129, the Polish KBN grant 221129102 (AAZ) and a *GRO* Fellowship (PSC).

REFERENCES

Boldt, E. 1987, Phys. Repts., 146, 215
Blumenthal, G. R., & Gould, R. J. 1970, Rev. Mod. Phys., 42, 237
Björnsson, G., & Svensson, R. 1991, ApJ, 371, L69
Coppi, P. S. 1992, MNRAS, 258, 657
Czerny, B., & Życki, P. T., ApJ, in press
Done, C. 1994, in preparation
Done, C., et al. 1992, ApJ, 395, 275
Fichtel, C. E., Simpson, G. A., & Thompson, D. J. 1978, ApJ, 222, 833
Fiore, F., Perola, G. C., Matsuoka, M., Yamauchi, M., & Piro, L. 1992, A&A, 262, 37
George, I. M., & Fabian, A. C. 1991, MNRAS, 249, 352
Ghisellini, G., Haardt, F., & Fabian, A. C. 1993, MNRAS, 263, L9
Ghisellini, G., Haardt, F., & Matt, G. 1994, MNRAS, 267, 743
Górecki, A., & Wilczewski, W. 1984, Acta Astr., 34, 141
Gruber, D. E. 1992, in The X-Ray Background, eds. X. Barcons & A. C. Fabian (Cambridge University Press), 44
Haardt, F.,& Maraschi, L. 1993, ApJ, 413, 507 (HM93)
Hasinger, G. 1992, in International Space Year (ESA ISY-3), 111
Inoue, H. 1989, in 23rd ESLAB Symp. on Two-Topics in X-Ray Astronomy (ESA SP-296), 783
Johnson, W. N., et al. 1994, in The Second Compton Symposium, ed. C. E. Fichtel et al. (New York: IAP), 515
Lahav, O, et al. 1993, Nature, 364, 693
Lightman, A. P., & White, T. R. 1988, ApJ, 335, 57
Lightman, A. P., & Zdziarski, A. A. 1987, ApJ, 319, 643
Madejski, G. M., et al. 1994, ApJ, submitted (M94)
Maisack, M., et al. 1993, ApJ, 407, L61
Nandra, K., & Pounds, K. 1994, MNRAS, 268, 405 (NP94)
Piccinotti, G., et al. 1982, ApJ, 253, 485
Piro, L., Yamauchi, M., & Matsuoka, M. 1990, ApJ, 360, L35
Pounds, K. A., Nandra, K., Stewart, G. C., George, I. M., & Fabian, A. C. 1990, Nature, 344, 132
Pozdnyakov, I. A., Sobol', I. M., & Sunyaev, R. A. 1977, Astr. Zh., 54, 1246 (Sov. Astr.–AJ, 21, 708)
Press, W. H., Teukolsky, S. A., Vetterling, W. T., & Flannery, B. P. 1992, Numerical Recipes, 2nd Ed. (Cambridge: Cambridge Univ. Press)
Rothschild, R. E., et al. 1983, ApJ, 269, 423
Sunyaev, R. A., & Titarchuk, L. G. 1980, A&A, 86, 121
Svensson, R. 1984, MNRAS, 209, 175
Svensson, R. 1987, MNRAS, 227, 403 (S87)
Svensson, R., & Zdziarski, A. A. 1994, ApJ, in press
Trombka, J. I., et al. 1977, ApJ, 212, 925
White, T. R., Lightman, A. P., & Zdziarski, A. A. 1988, ApJ, 331, 939
Zdziarski, A. A. 1985, ApJ, 289, 514 (Z85)
Zdziarski, A. A. 1986, ApJ, 303, 94
Zdziarski, A. A., Lightman, A. P., & Maciołek-Niedźwiecki, A. 1993, ApJ, 414, L93

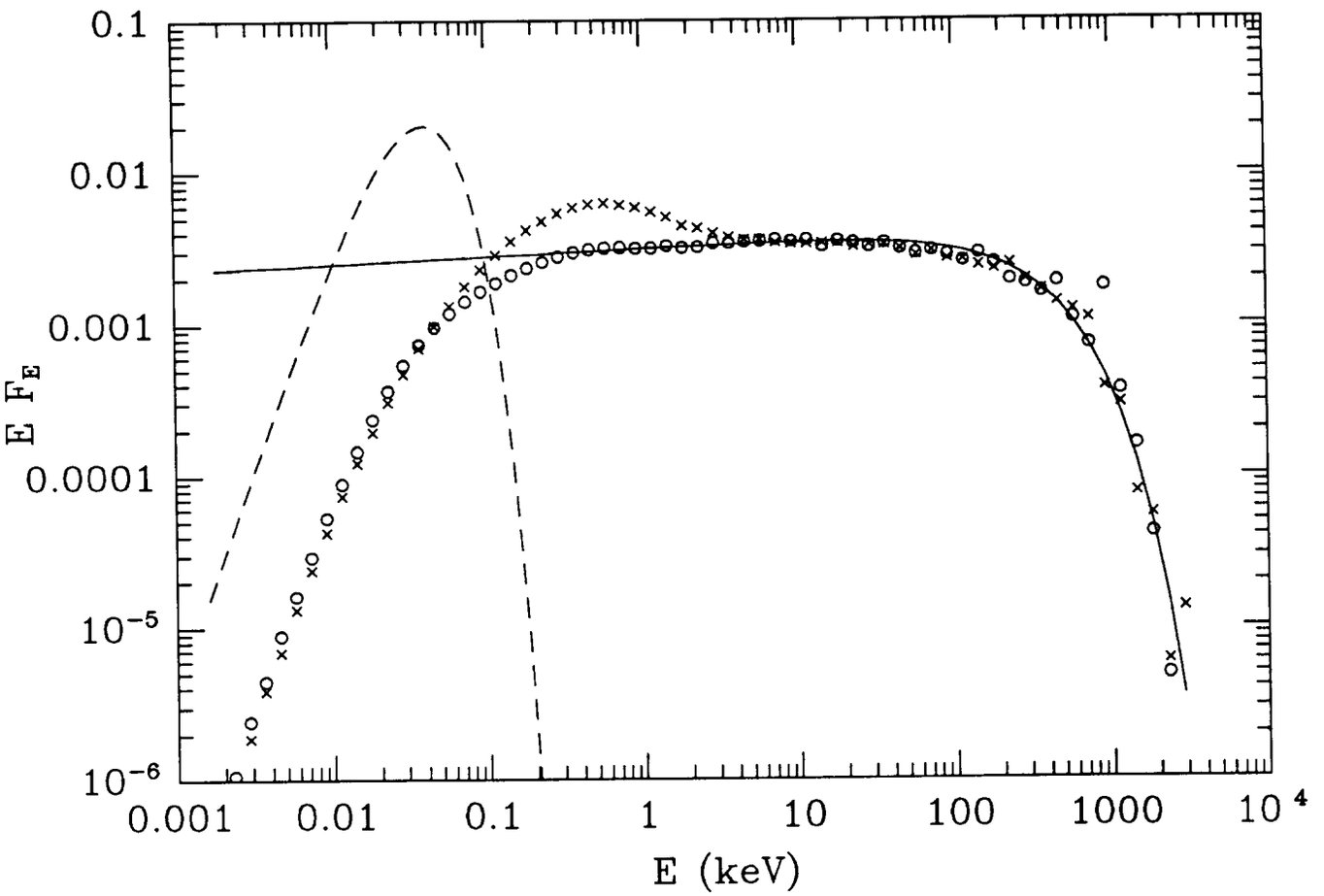

Figure 1

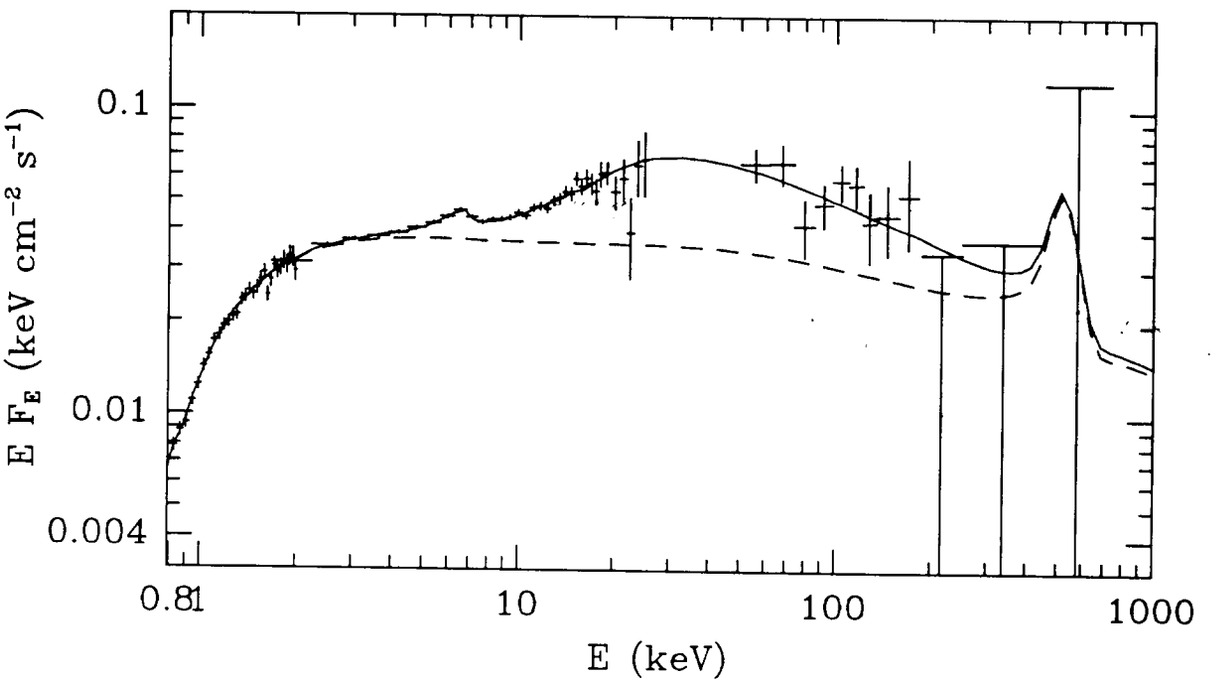

Figure 2

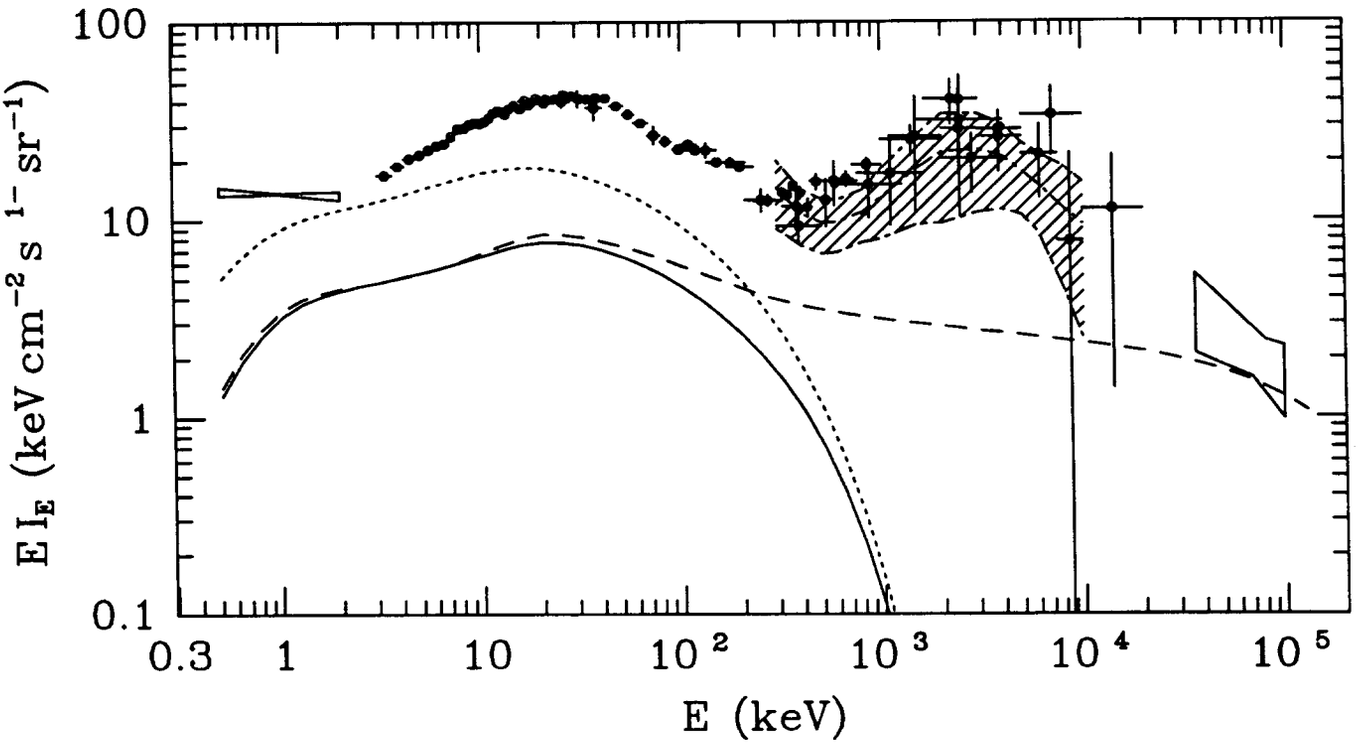

Figure 3